DEEP LEARNING-BASED SCENE CLASSIFICATION OF VERY HIGH-RESOLUTION SATELLITE IMAGERY FOR POST-EARTHQUAKE DAMAGE ASSESSMENT: A CASE STUDY OF THE 2023 KAHRAMANMARAŞ EARTHQUAKES

D. Ilmak [1], M. C. Iban [2] *, D. Z. Seker [3]

[1] Dept. of Remote Sensing and GIS, Mersin University, 33343, Mersin, Türkiye – doguilmak@gmail.com
[2] Dept. of Geomatics Engineering, Mersin University, 33343, Mersin, Türkiye – caniban@mersin.edu.tr
[3] Dept. of Geomatics Engineering, Istanbul Technical University, 80626, Istanbul, Türkiye – seker@itu.edu.tr

KEY WORDS: Deep Learning, Scene Classification, Satellite Imagery, Remote Sensing, Earthquakes, Damage Assessment.

ABSTRACT:

Following the devastating earthquakes in Kahramanmaraş province, Türkiye, on February 6, 2023, which resulted in the loss of over 50,000 lives and damage to more than 84,000 buildings, the pressing need for efficient damage assessment and response became apparent. Traditional on-site assessments are time-consuming and perilous. Most existing research leans towards segmentation and object detection methods for earthquake damage assessment using remotely sensed data, which demand substantial training data, computational resources, and time. A more practical approach can be classifying image patches to identify earthquake-affected areas with damaged buildings. This scene classification method categorizes image patches based on their content. Remote sensing scene classification assigns labels to such images using deep learning various algorithms. In this work, we developed a fully automated system utilizing Maxar's very high-resolution post-earthquake satellite imagery to classify and map the scenes (image patches) involving collapsed and non-collapsed buildings in Antakya and Iskenderun city centers. Our approach involved two key scene classifiers: Classifier #1, employing deep learning models like ResNet-101, effectively detected building presence within the image scene with remarkable accuracy (99.17%). This classifier served as the foundation for identifying the scenes involving buildings for entire city in order to filter the non-urban land use. Then, Classifier #2, classified building scenes into collapsed and non-collapsed categories. The DenseNet-121 model excelled, achieving an accuracy of 93.33% in this task. In the end, Classifier #2 categorized 2,429 non-collapsed and 449 collapsed scenes in Antakya and 2,291 non-collapsed and 290 collapsed scenes in Iskenderun.

1. INTRODUCTION

Earthquakes, which are destructive natural disasters, cause significant destruction to communities and infrastructure all around the world. One major concern is the damage caused to buildings in cities. To address this issue effectively, it is crucial to gather information about the size of the affected area, the extent of the damage, how many buildings have collapsed, the severity of damage in the affected area, and the specific types of damage to individual buildings. This information is essential for organizing urgently needed rescue efforts and planning the reconstruction process after a devastating earthquake (Dong and Shan, 2013). While it is true that accurately assessing the damage to individual buildings requires experts who can inspect both the inside and the outside, it is important to recognize the challenges in this process (Matin and Pradhan, 2022). This kind of evaluation takes a lot of time and resources and can be dangerous because it requires people to physically go to the affected area. Additionally, when earthquakes happen in large cities, it is nearly impossible to inspect every building quickly enough to meet the urgent needs of rescue operations and damage control (Shi et al., 2021).

On the other hand, satellite images give a complete and up-to-date look at the areas affected by the disaster, making it much quicker and more efficient to understand the damage. Having the ability to quickly get high-resolution satellite images right after an earthquake is crucial for helping rescue teams, allocating resources, and planning how to respond to the disaster (Munawar et al., 2022). Furthermore, the repetitive and continuous nature of satellite imaging guarantees that post-disaster assessment can be carried out at regular intervals, enabling the tracking of recovery progress and identification of areas that may necessitate additional support (Shafapourtehrany et al., 2023).

On February 6, 2023, a very devastating earthquake with a magnitude of 7.8 hit the southern part of Kahramanmaraş province in Türkiye. Nine hours later, there was another strong earthquake with a magnitude of 7.5 in the central part of the same province. These earthquakes caused a terrible disaster, with more than 84,000 buildings either collapsing or suffering severe damage and more than 50,000 people lost their lives in both Türkiye and Syria. Among the hardest-hit areas was Hatay Province, which experienced extensive damage. The earthquakes caused varying degrees of destruction to most of the masonry structure buildings in Antakya and surrounding cities in the Hatay Province, including wall cracking, partial collapses, and complete building failures (Tao et al., 2023).

The central objective of this research revolves around the development of a fully automated system geared towards the classification of areas within high-resolution satellite images that encompass collapsed buildings. To facilitate the training and subsequent evaluation of the deep learning models, we meticulously curated an annotated dataset of Maxar satellite images covering Antakya and Iskenderun Cities in the Hatay Province.

Initially, this dataset was meticulously annotated to differentiate between scenes "with buildings" and those "without buildings." Subsequently, predictive algorithms were employed to identify scenes featuring buildings, thereby distinguishing them from scenes devoid of any architectural structures. Subsequent to this classification, scenes categorized as containing individual

* Corresponding author

buildings underwent another meticulous annotation. In this phase, the labels pertained to scenes that either featured "collapsed buildings" or "non-collapsed buildings." This distinction was essential in accentuating the presence or absence of collapsed structures within the scene.

It is worth noting that the detection of boundaries for the remnants of collapsed buildings presents a distinct challenge, primarily due to the unique patterns exhibited by completely collapsed structures, such as pancake collapses. In the context of Antakya and Iskenderun Cities, where a substantial number of buildings were severely impacted by the earthquake, this becomes an especially pertinent consideration. Consequently, the accurate geolocation of city patches featuring collapsed buildings assumes heightened significance, particularly in the context of humanitarian aid efforts immediately following the mainshock event.

In pursuit of this overarching goal, it is required to ensure that the spatial resolution of the data under consideration attains a level of granularity sufficient to differentiate between architectural structures and various other features present within the urban landscape. In the context of similar research endeavors, the datasets frequently employed can be categorized into four distinct classes, namely: (1) optical data, (2) synthetic aperture radar (SAR) data, (3) light detection and ranging (LiDAR) data, and (4) ancillary data. It is noteworthy that the ancillary data category encompasses cartographic representations derived from geographic information system (GIS) datasets procured via remote sensing techniques, as well as field-based building damage assessments conducted in situ (Dong and Shan, 2013).

Many research studies have looked into various ways to use remote sensing images to understand how earthquakes damage buildings. These methods generally fall into two categories. (1) *Multi-temporal assessment:* This means looking at changes in images over time to see damage. The traditional way is to compare images before and after an earthquake to spot differences in things like texture and brightness (Adriano et al., 2019). While these methods work well, they need both pre-earthquake and post-earthquake images, which can be a challenge in real-life situations where such data might not be available (Matin and Pradhan, 2022). (2) *Single-post-image assessment:* In this approach, researchers use only one image taken after the earthquake to figure out the damage to buildings. This method does not rely on having images from before the earthquake. These methods mainly rely on gathering statistics from image objects, which includes texture and shape. (Karimzadeh and Matsuoka, 2018; Matin and Pradhan, 2022).

Apart from feature-based classification (Vu, 2012) and conventional machine learning methods (Chauhan and Singh, 2018), some studies have explored the realm of deep learning techniques, which entail the identification of collapsed structures through patch-based analysis of single post-event images. In recent years, deep learning methodologies have emerged as the forefront techniques in the domain of machine learning, garnering recognition as some of the most prevalent methods for extracting valuable information from remote sensing imagery (Ozturk et al., 2023; Sariturk et al., 2022). These approaches are fundamentally rooted in neural networks, and their ascendancy within the field can be attributed to their remarkable capacity to autonomously learn intricate features ranging from low-level to high-level representations directly from raw image data. Consequently, this reduces the need for user intervention in the selection of arbitrary image features, setting deep learning apart from conventional machine learning techniques (Wang et al., 2022).

Within the realm of utilizing optical remote sensing data to identify earthquake-induced damage in affected regions, three principal paradigms have been extensively documented in the literature: *detection*, *segmentation*, and *classification* (Matin and Pradhan, 2022). Segmentation models entail the meticulous labelling of each pixel within an image, adhering to predefined damage level guidelines (Wang et al., 2023). In contrast, detection models necessitate the labelling of buildings in accordance with these damage level guidelines during the training phase (Jing et al., 2022). Meanwhile, the classification approach involves the labelling of individual image patches based on the presence or absence of damaged buildings within them.

The existing body of research predominantly leans towards segmentation and object detection methodologies for earthquake damage assessment using remotely sensed datasets. Nonetheless, these approaches impose significant demands in terms of training data volume, computational resources, and time-intensive training processes. Therefore, a more practical approach might be to use a method that classifies the scenes (image patches) to identify areas in large earthquake-affected regions where buildings are damaged. This scene classification methodology aims to categorize image patches based on their inherent scene content. Remote sensing scene classification involves the assignment of specific labels to remote sensing scene images, accomplished through the application of various algorithmic techniques. Deep learning has been widely employed in remote sensing scene classification, yielding remarkable successes. Notably, the majority of these endeavors rely on extensive, large-scale remote sensing datasets, often encompassing thousands of image patches for each distinct category, to effectively train neural network models (Yuan et al., 2023). Additionally, GIS data has proven instrumental in delineating the boundaries of building blocks or scenes that are to be subjected to classification. For instance, a notable study by Ye et al. (2016) employed block information derived from urban road vector data in post-earthquake Gaofen-1 images. This approach facilitated the construction of a classification model, with building blocks as its fundamental units. The results of this study demonstrated high classification accuracy in assessing the damage degree of groups of buildings. Another noteworthy contribution by Ma et al. (2020) introduced an improved Convolutional Neural Network (CNN) architecture, Inception V3, which seamlessly integrated remote sensing imagery with block vector data for evaluating the damage degree of building groups within post-earthquake remote sensing images.

2. METHOD

2.1 Scene Classification Scheme

The scene classification scheme of this study is two-fold:

Classifier #1: The initial step involves the creation of a deep learning model, employing a variety of architectural frameworks. The primary objective of this model is to undertake the detection of buildings within the given image patch. To accomplish this, the model is meticulously trained on a dataset comprising annotated image patches, enabling it to make precise determinations regarding the presence or absence of buildings. This binary classification task revolves around two distinct classes, each signifying either the existence or absence of buildings within the image patches. This process allows for

the effective filtration of image patches devoid of any buildings, taking into account the inclusion of large non-urban areas within the Maxar images.

Classifier #2, building upon the insights gained from the optimal model developed for Classifier #1, focuses on a subsequent stage of the analysis. Here, we embark on the task of refining the predictions made by Classifier #1, specifically targeting the subset of scenes that have been classified as *building scenes*. In this phase, we focus on the creation of another deep learning model, leveraging the same architectural frameworks as utilized in Classifier #1. The primary objective of this model is to categorize image patches of buildings into two distinct categories: those that depict collapsed structures and those that do not. This classification is underpinned by meticulously annotated image patches, allowing us to draw a clear distinction between areas that have undergone structural collapse and those that have remained intact.

2.2 Data Preparation

In the aftermath of the Kahramanmaraş earthquake sequence, Maxar Technologies furnished very high-resolution satellite imagery captured on February 8, 2023. This imagery resource, made accessible through the Maxar Open Data Program (2023), played a crucial role in facilitating emergency preparedness, risk evaluation, monitoring, emergency response coordination, damage assessment, and post-disaster recovery endeavors. Notably, the Maxar Open Data catalog offers versatile data formats, including GeoJSON, CSV, and MosaicJSON, thereby affording convenience for data utilization in various programming languages. In our research study, we used an interactive mapping repository, created by Wu (2023), to access and visualize the GeoDataFrame specific to the Kahramanmaraş Earthquake catalog, which encompasses Maxar satellite imagery information. The GeoDataFrame provides URLs for each individual image, enabling seamless retrieval and subsequent downloading of these images in TIFF format to the working directory for further analysis and utilization.

In our research, we deliberately designated two contiguous Maxar images (with RGB bands of 0.5 m resolution) characterized by quadkeys 031133023302 and 031133023303. These images, each spanning a substantial area of the Antakya City Center, boasted dimensions of 17408×17408 pixels. As depicted in Figure 1, a deliberate partitioning strategy was employed. This entailed the allocation of two discrete regions for training purposes and an additional two distinct areas designated for testing, facilitating the annotation of labels essential for both classifiers. Furthermore, a sole validation area was exclusively set aside for the purpose of model validation. *Training Area 1* is situated within the city center, characterized by a dense concentration of buildings. Conversely, *Training Area 2* is positioned outside the urban confines, showcasing non-building land use patterns (including parks, forests, agricultural lands etc.). Both of these delineated regions, denoted by red coloring, were chosen to serve as the basis for selecting and annotating training samples essential for the building/non-building classifier, referred to as Classifier #1. In the context of selecting and annotating training samples for the collapsed/non-collapsed classifier, denoted as Classifier #2, we exclusively leveraged *Training Area 1*. A similar procedure was applied to our test areas, highlighted in yellow. *Testing Area 1* is located within a densely inhabited zone, while Testing Area 2 occupies a non-inhabited zone. These test areas play a critical role in evaluating the predictive performance of Classifier #1. However, *Testing Area 1* is solely utilized to assess the predictive capabilities of Classifier #2. For validation purposes, an area demarcated in blue was selected, characterized by a blend of both inhabited and non-inhabited land use. In summation, our efforts yielded a collection of training, testing, and validation image patches. The dataset for training Classifier #1 comprised 200 samples for each class (‘Building’ and ‘Non-Building’) with 90 samples allocated for validation and 60 for testing in each class. In total, Classifier #1 utilized 400 samples for training, 180 for validation, and 120 for testing. Classifier #2, on the other hand, utilized 200 samples for training in each class (‘Collapsed’ and ‘Non-Collapsed’), with 90 samples designated for validation and 60 for testing in both classes. Consequently, Classifier #2 also utilized a total of 400 samples for training, 180 for validation, and 120 for testing. The image patches were standardized to a size of 224×224 pixels, ensuring consistent inputs for our model evaluations.

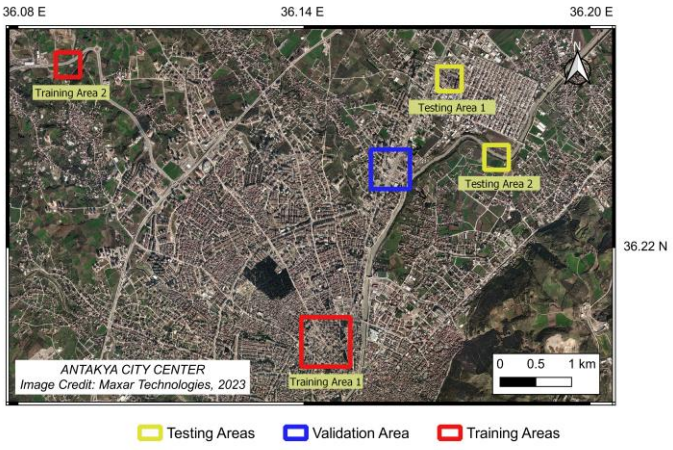

Figure 1. Antakya City Center and the areas comprising training, testing, and validation scenes

2.3 Deep Learning Models

Given their demonstrated efficacy in previous instances like the ImageNet Large Scale Visual Recognition Challenge, well-established architectures were employed, specifically VGG (16 and 19), MobileNetV2, ResNet (50, 50V2, 101), and DenseNet (121 and 169), for both classifiers. To ensure comprehensive model training, the number of training epochs was set at 32 for

Classifier #1 and 64 for Classifier #2. Batch sizes for training, validation, and testing phases were configured as 8, 4, and 2, respectively. The activation function used was softmax, and the loss function was categorical_crossentropy. The models were trained using Google Colab's T4 GPU, offering 40 cores, 16 GB GPU memory, 12 GB RAM, and a maximum memory bandwidth of 300 GB/sec.

ResNet tackles the vanishing gradient issue with skip-connections, allowing earlier layer outputs to influence later ones, aiding gradient flow (He et al., 2016). We employ ResNet50, ResNet50V2, and ResNet101, tailored to various depths. VGG features increasing depth via stacked convolutional layers, with 3x3 filters, ReLU activation, batch normalization, and max-pooling. VGG-16 and VGG-19, with 16 and 19 weight layers respectively, provide deeper representations (Simonyan and Zisserman, 2014). DenseNet fosters information flow by densely connecting layers. Each convolutional layer links to all previous ones, followed by ReLU and batch normalization. DenseNet-121 and DenseNet-169 offer progressively deeper features (Huang et al., 2017). MobileNet optimizes for efficiency with MobileNetv2 using depthwise separable convolutions, suitable for resource-constrained devices, while maintaining accuracy.

2.4 Performance Evaluation

To evaluate classifier performance, essential metrics are utilized. True Positives (tp) indicate accurate classifications of buildings and collapsed scenes. True Negatives (tn) denote correct identifications of non-building, non-collapsed scenes. False Positives (fp) and False Negatives (fn) signify misclassifications. A confusion matrix is employed for evaluation, crucial for quantifying performance, to compute following metrics: *Accuracy* provides an overall measure of how well a classification model correctly predicts both positive and negative instances. The formula for accuracy is calculated as (tp + tn) / (tp + fn + fp + tn). *Precision* assesses the accuracy of positive predictions made by the model, focusing on the instances it identifies as positive. The formula for precision is tp / (tp + fp). *Recall* evaluates the model's ability to correctly identify positive instances among all actual positive instances. The formula for recall is tp / (tp + fn). The *F-1 Score* is the harmonic mean of precision and recall, providing a balanced measure of a model's overall performance. The formula for the F-1 Score is (2 * Precision * Recall) / (Precision + Recall). Evaluation metrics also encompass the Receiver Operator Characteristic (ROC) curve and Area under the ROC Curve (AUC). ROC curves leverage probability curves to assess classifier performance. Higher AUC values denote superior accuracy, with values exceeding 0.9 aligning with established benchmarks.

2.5 Predictive Inference

Following rigorous training and evaluation, the top-performing models were selected for predictive inference. The trained classifiers play a crucial role in predicting building and collapsed scenes in Antakya City and its neighboring Iskenderun (image quadkey: 031133021303), both affected by the Kahramanmaraş Earthquake sequence. Utilizing these classifiers, image patches across these cities are systematically assessed, representing a unique approach that relies on relatively limited annotated data. This strategic step enhances the ability to monitor and analyze urban areas, resulting in valuable insights for post-earthquake damage assessment.

3. RESULTS

3.1 Classifier #1

Classifier #1 is designed with the specific objective of identifying the existence of buildings within the image patch under consideration. As detailed in Table 1, it is evident that all employed model architectures have demonstrated commendable performance in the classification of both building and non-building scenes. Notably, each of these models has achieved a minimum accuracy of 0.87, a precision of 0.78, a recall of 0.95, and an F-1 score of 0.86.

However, among the array of models assessed, the ResNet-101 model has exhibited a remarkable level of proficiency, consistently outperforming its counterparts across all metrics. With an accuracy score of 0.9917, precision at 0.9833, perfect recall (1.000), and an impressive F-1 score of 0.9916, the ResNet-101 model has emerged as the frontrunner in terms of classification prowess. These results highlight the model's effectiveness in detecting buildings within the image patch, affirming its importance in our classification framework. Most models achieved a perfect recall score of 1.000, ensuring no false negatives in their predictions.

	Architecture	Performance Metrics			
		Accuracy	Precision	Recall	F-1 Score
Classifier #1	DenseNet-121	0.9583	0.9167	1.0000	0.9565
	DenseNet-169	0.9167	0.8333	1.0000	0.9091
	MobileNetv2	0.9750	0.9500	1.0000	0.9744
	ResNet-50	0.9333	0.8667	1.0000	0.9286
	ResNet-50v2	0.9583	0.9167	1.0000	0.9565
	ResNet-101	**0.9917**	**0.9833**	**1.0000**	**0.9916**
	VGG-16	0.8750	0.7833	0.9592	0.8624
	VGG-19	0.8833	0.7833	0.9792	0.8704
Classifier #2	DenseNet-121	**0.9333**	**1.0000**	**0.8824**	**0.9375**
	DenseNet-169	0.8833	1.0000	0.8108	0.8955
	MobileNetv2	0.7000	1.0000	0.6250	0.7692
	ResNet-50	0.7750	0.7667	0.7797	0.7731
	ResNet-50v2	0.9000	0.9500	0.8636	0.9048
	ResNet-101	0.7500	0.5833	0.8750	0.7000
	VGG-16	0.8750	1.0000	0.8000	0.8889
	VGG-19	0.8583	0.9833	0.7867	0.8741

Table 1. Performance of Architectures Used for Classifier #1 and #2

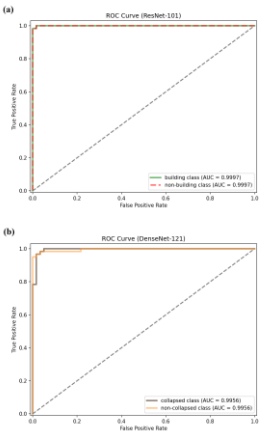

Figure 2. (a) ROC Curve of Classifier #1 (ResNet-101) and (b) Classifier #2 (DenseNet-121)

Furthermore, as depicted in Figure 2(a), plotted ROC curves and AUC values (0.9997) show that ResNet-101 model can be considered successful in terms of classifying the buildings and non-building samples.

Figure 3 illustrates Classifier #1's prediction outcomes with the ResNet-101 model on select test samples. In Figure 3(a), a correctly identified building scene (tp) is shown. Figure 3(b) displays a misclassified non-building scene (fn), while Figure 3(c) exhibits an accurately recognized non-building scene (tn).

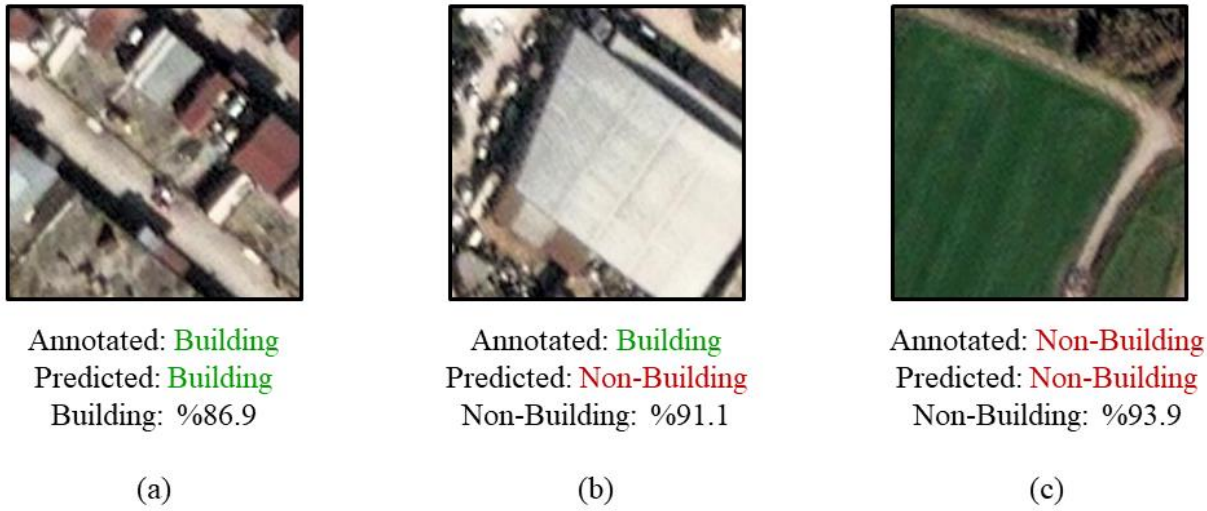

Figure 3. Predictions on Test Samples of Classifier #1

3.2 Classifier #2

Classifier #2 was specifically designed to identify collapsed buildings within the image patch under analysis. As outlined in Table 1, most of the employed model architectures have exhibited commendable performance in classifying both collapsed and non-collapsed scenes. It is noteworthy that each of these models achieved a minimum accuracy of 0.70, a precision of 0.58, a recall of 0.63, and an F-1 score of 0.70. However, among the various models evaluated, the DenseNet-121 model consistently stood out, surpassing its peers across all metrics. With an impressive accuracy score of 0.9333, perfect precision at 1.000, a recall of 0.8824, and an F-1 score of 0.9375, the DenseNet-121 model emerged as the top performer in terms of classification capability. These results underscore the effectiveness of this model architecture in successfully detecting collapsed structures within the image patch, solidifying its prominence within our classification framework.

Additionally, as illustrated in Figure 2(b), the plotted ROC curves and the AUC value of 0.9956 demonstrate that the DenseNet-121 model can be considered highly effective in classifying collapsed and non-collapsed samples.

Figure 4 presents the prediction results of Classifier #2 utilizing the DenseNet-121 model on a selection of test samples. In Figure 4(a), we can see two samples correctly classified as collapsed scenes (tp). In Figure 4(b), two samples are depicted that were incorrectly classified as collapsed scenes (fp). Lastly, in Figure 4(c), we highlight two samples that were correctly identified as non-collapsed scenes (tn).

3.3 Predictive Inference Results

We conducted predictive inference using trained classifiers to identify building/non-building scenes and collapsed/non-collapsed scenes across the entire Antakya and Iskenderun city centers. This endeavor had two primary objectives: first, to quantify the number of scenes within each category, and second, to create maps based on these categories. As per the predictions made by Classifier #1, the map depicting building/non-building scenes is presented in Figure 5(a) for Antakya and Figure 6(a) for Iskenderun. Correspondingly, Classifier #2's predictions, which illustrate collapsed/non-collapsed scenes, can be found in Figure 5(b) for Antakya and Figure 6(b) for Iskenderun. Based on these predictions, Classifier #2, on the other hand, categorized these scenes into 2,429 non-collapsed and 449 collapsed scenes in Antakya, and 2,291 non-collapsed and 290 collapsed scenes in Iskenderun (see Figure 7).

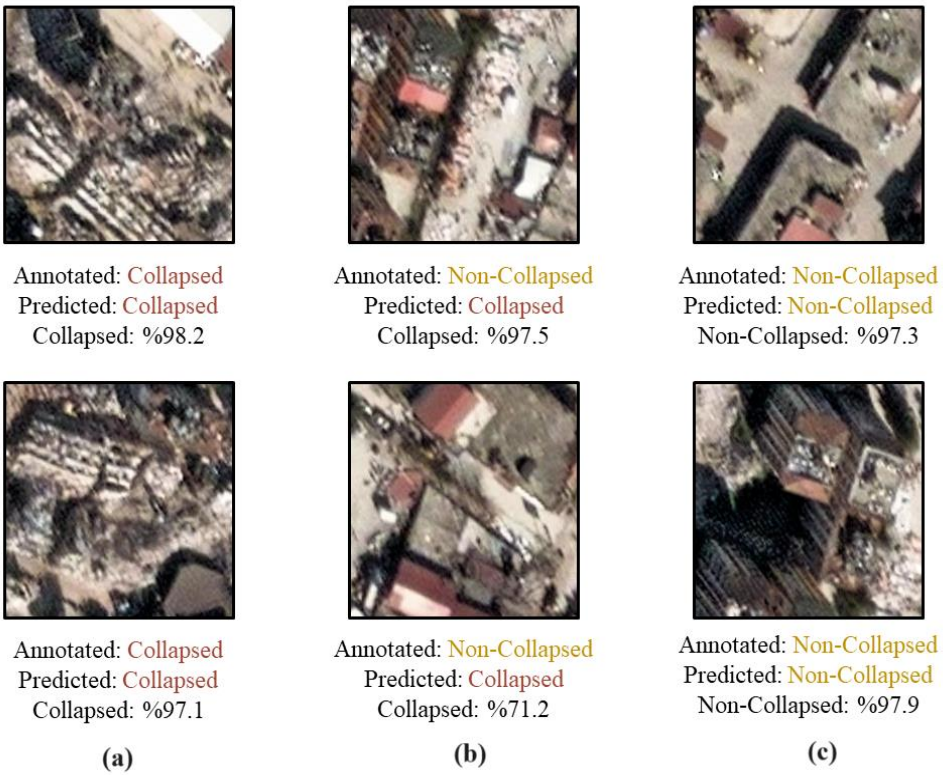

Figure 4. Predictions on Test Samples of Classifier #2

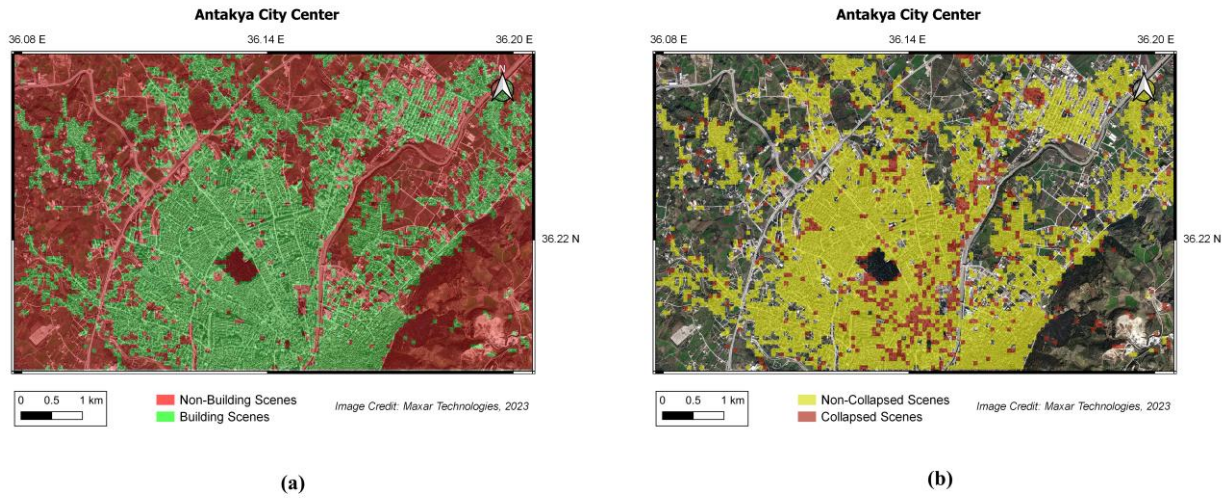

Figure 5. (a) Predictions of Classifier #1 on each scene in Antakya (ResNet-101), (b) Predictions of Classifier #2 on each building scene in Antakya (DenseNet-121)

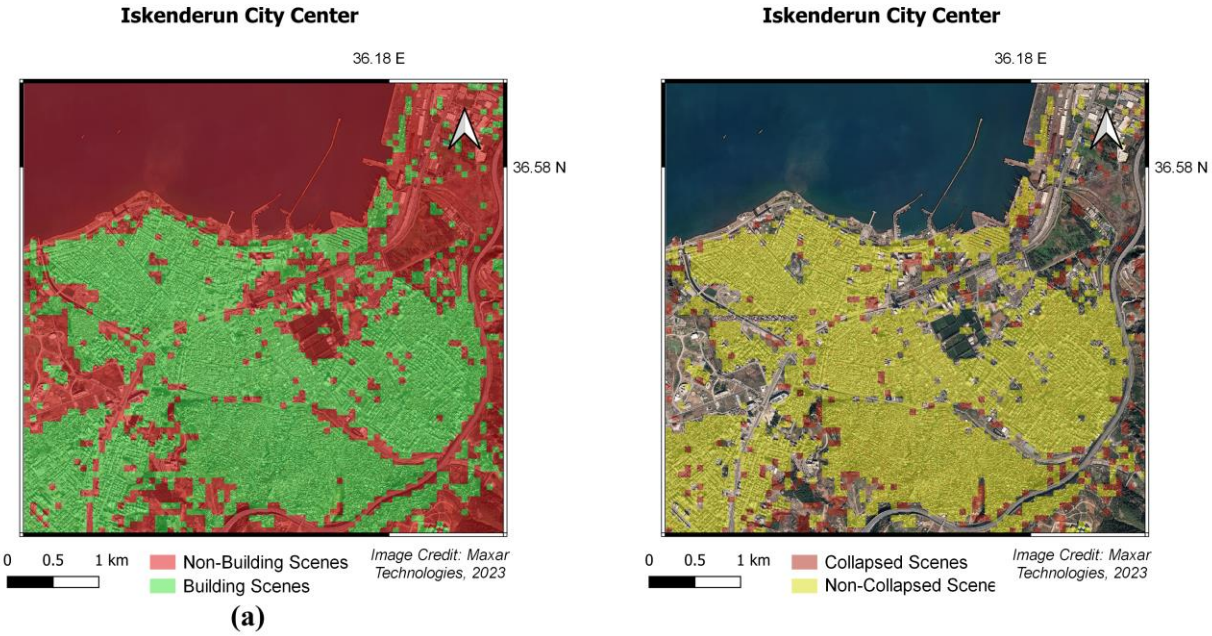

Figure 6. Predictions for Iskenderun (a) Classifier #1 (ResNet-101), (b) Classifier #2 (DenseNet-121)

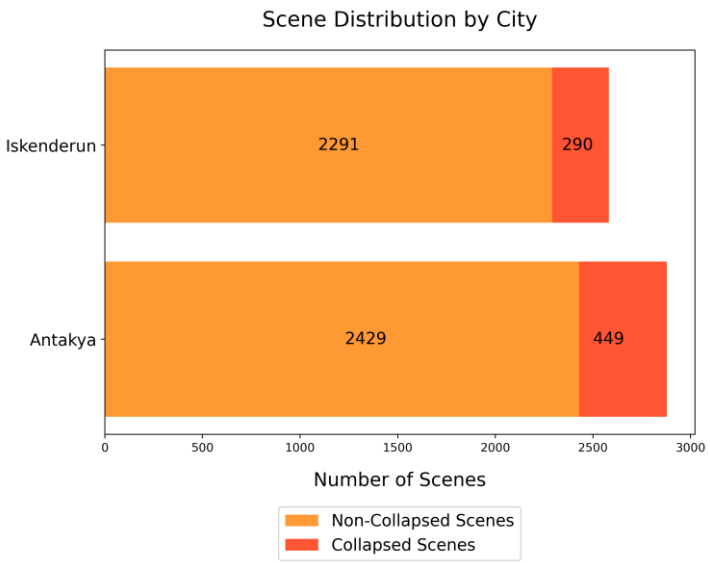

Figure 7. Scene Distribution by City

4. DISCUSSION & CONCLUSION

In this study, we designed a fully automated system that utilizes high-resolution post-earthquake satellite imagery from Maxar to classify and map scenes, including both collapsed and non-collapsed buildings in the city centers of Antakya and Iskenderun. Classifier #1, utilizing deep learning models such as ResNet-101, demonstrated remarkable accuracy in detecting the presence of buildings within image scenes, achieving a 99.17% accuracy. This classifier served as the foundation for identifying scenes with buildings across the entire city to filter out non-urban areas. Subsequently, Classifier #2 was employed to categorize building scenes into collapsed and non-collapsed groups, with the DenseNet-121 model achieving an accuracy of 93.33% in this task. Ultimately, Classifier #2 identified 2,429 non-collapsed scenes and 449 collapsed scenes in Antakya, along with 2,291 non-collapsed scenes and 290 collapsed scenes in Iskenderun. DenseNet-121 being the best model for this scene classification task could be attributed to several reasons. First, DenseNet is known for its dense connectivity pattern, which allows each layer to receive input from all preceding layers. This dense connectivity helps in feature reuse and learning more complex representations, which can be beneficial for scene classification tasks. Second, DenseNet architectures often have fewer parameters compared to traditional architectures like VGG and ResNet. This parameter efficiency can be crucial, especially when the analyst has limited computational resources or a smaller dataset.

The practicality of scene classification methods, as highlighted in the literature review, cannot be overstated. By swiftly classifying image patches based on their inherent content, scene classification offers a pragmatic and efficient approach to identifying earthquake-affected areas, especially in large-scale disaster scenarios. This streamlined approach, supported by the remarkable successes of deep learning in remote sensing scene classification, holds promise as a vital component of rapid response efforts following an earthquake event. By simplifying the labeling process and expediting damage assessment, scene classification emerges as a valuable tool for aiding and rescue activities in the aftermath of earthquakes.

A limitation of our study is the challenge posed by varying angles in the imagery, leading to ambiguity in damage identification. Hence, Classifier #2 does not assess damage extent due to these constraints. Future research should prioritize improving building footprint datasets and obtaining ample labeled data for specific disaster types. Furthermore, investigating deep learning models for building damage assessment, especially through unsupervised domain adaptation, holds promise. This is critical since disaster scenarios often lack labeled data in the target domain.

CODE

The code employed in this project is available at:

https://github.com/geoaihub/GeoAdvances-EQ-Scene-Classification-2023-Kahramanmaras

REFERENCES

Adriano, B., Xia, J., Baier, G., Yokoya, N., Koshimura, S., 2019: Multi-Source Data Fusion Based on Ensemble Learning for Rapid Building Damage Mapping during the 2018 Sulawesi Earthquake and Tsunami in Palu, Indonesia. *Remote Sensing* 11(7), 886.

Chauhan, N.K., Singh, K., 2018. A Review on Conventional Machine Learning vs Deep Learning. *2018 International Conference on Computing, Power and Communication Technologies (GUCON)*. 347–352.

Dong, L., Shan, J., 2013: A comprehensive review of earthquake-induced building damage detection with remote sensing techniques. *ISPRS Journal of Photogrammetry and Remote Sensing* 84, 85–99.

He, K., Zhang, X., Ren, S., Sun, J., 2016: Deep residual learning for image recognition. In *Proceedings of the IEEE Conference on Computer Vision and Pattern Recognition*, pp. 770-778.

Huang, G., Liu, Z., Van Der Maaten, L., Weinberger, K. Q., 2017: Densely connected convolutional networks. In *Proceedings of the IEEE Conference on Computer Vision and Pattern Recognition*, pp. 4700-4708.

Jing, Y., Ren, Y., Liu, Y., Wang, D., Yu, L., 2022: Automatic Extraction of Damaged Houses by Earthquake Based on Improved YOLOv5: A Case Study in Yangbi. *Remote Sensing* 14(2), 382.

Karimzadeh, S., Matsuoka, M., 2018: Building Damage Characterization for the 2016 Amatrice Earthquake Using Ascending–Descending COSMO-SkyMed Data and Topographic Position Index. *IEEE Journal of Selected Topics in Applied Earth Observations and Remote Sensing* 11, 2668–2682.

Ma, H., Liu, Y., Ren, Y., Wang, D., Yu, L., Yu, J., 2020: Improved CNN Classification Method for Groups of Buildings Damaged by Earthquake, Based on High Resolution Remote Sensing Images. *Remote Sensing* 12(2), 260.

Matin, S.S., Pradhan, B., 2022: Challenges and limitations of earthquake-induced building damage mapping techniques using remote sensing images-A systematic review. *Geocarto International* 37(21), 6186–6212.

Maxar, 2023. Open Data Program. maxar.com/open-data (18 September 2023).

Munawar, H.S., Mojtahedi, M., Hammad, A.W.A., Kouzani, A., Mahmud, M.A.P., 2022: Disruptive technologies as a solution for disaster risk management: A review. *Science of The Total Environment* 806(3), 151351.

Ozturk, O., Isik, M.S., Kada, M., Seker, D.Z., 2023: Improving Road Segmentation by Combining Satellite Images and LiDAR Data with a Feature-Wise Fusion Strategy. *Applied Sciences* 13(10), 6161.

Sariturk, B., Seker, D.Z., Ozturk, O., Bayram, B., 2022: Performance evaluation of shallow and deep CNN architectures on building segmentation from high-resolution images. *Earth Science Informatics* 15, 1801–1823.

Simonyan, K., Zisserman, A., 2014: Very deep convolutional networks for large-scale image recognition. *arXiv preprint* arXiv:1409.1556.

Shafapourtehrany, M., Batur, M., Shabani, F., Pradhan, B., Kalantar, B., Özener, H., 2023: A Comprehensive Review of Geospatial Technology Applications in Earthquake Preparedness, Emergency Management, and Damage Assessment. *Remote Sensing* 15(7), 1939.

Shi, L., Zhang, F., Xia, J., Xie, J., Zhang, Z., Du, Z., Liu, R., 2021: Identifying Damaged Buildings in Aerial Images Using the Object Detection Method. *Remote Sensing* 13(21), 4213.

Tao, W., Jie, C., Yujiang, Z., Xiaoqing, W., Xuchuan, L., Xiaoting, W., Qingxue, S., 2023: Preliminary investigation of building damage in Hatay under February 6, 2023 Turkey earthquakes. *Earthquake Engineering and Engineering Vibration* (article in press).

Vu, T.T., 2012. Rapid Disaster Damage Estimation. *The International Archives of the Photogrammetry, Remote Sensing and Spatial Information Sciences* XXXIX-B8, 65–69. doi.org/10.5194/isprsarchives-XXXIX-B8-65-2012

Wang, P., Bayram, B., Sertel, E., 2022: A comprehensive review on deep learning based remote sensing image super-resolution methods. *Earth-Science Reviews* 232, 104110.

Wang, Y., Jing, X., Xu, Y., Cui, L., Zhang, Q., Li, H., 2023: Geometry-guided semantic segmentation for post-earthquake buildings using optical remote sensing images. *Earthquake Engineering & Structural Dynamics* 52, 3392–3413.

Ye, X., Wang, J., Qin, Q., 2016: Damaged building detection based on GF-1 satellite remote sensing image: A case study for Nepal MS8.1 earthquake. *Acta Seismologica Sinica* 38, 477–485.

Yuan, Z., Tang, C., Yang, A., Huang, W., Chen, W., 2023: Few-Shot Remote Sensing Image Scene Classification Based on Metric Learning and Local Descriptors. *Remote Sensing* 15(3), 831.